AMERICAN SOCIETY FOR MICROBIOLOGY | mSphere®

RESEARCH ARTICLE
Host-Microbe Biology

Internalization of Erythrocyte Acylpeptide Hydrolase Is Required for Asexual Replication of *Plasmodium falciparum*

Rubayet Elahi,[a] Christie Dapper,[a] Michael Klemba[a]

[a]Department of Biochemistry, Virginia Tech, Blacksburg, Virginia, USA

ABSTRACT The human malaria parasite *Plasmodium falciparum* causes disease as it replicates within the host's erythrocytes. We have found that an erythrocyte serine hydrolase, acylpeptide hydrolase (APEH), accumulates within developing asexual parasites. Internalization of APEH was associated with a proteolytic event that reduced the size of the catalytic polypeptide from 80 to 55 kDa. A triazole urea APEH inhibitor, termed AA74-1, was employed to characterize the role of parasite-internalized APEH. In cell lysates, AA74-1 was a potent and highly selective inhibitor of both host erythrocyte and parasite-internalized APEH. When added to cultures of ring-stage parasites, AA74-1 was a poor inhibitor of replication over one asexual replication cycle; however, its potency increased dramatically after a second cycle. This enhancement of potency was not abrogated by the addition of exogenous isopentenyl pyrophosphate, the sole essential product of apicoplast metabolism. High-potency inhibition of parasite growth could be effected by adding AA74-1 to schizont-stage parasites, which resulted in parasite death at the early trophozoite stage of the ensuing replication cycle. Analysis of APEH inhibition in intact cultured cells revealed that host erythrocyte APEH, but not the parasite-internalized APEH pool, was inhibited by exogenous AA74-1. Our data support a model for the mode of parasiticidal activity of AA74-1 whereby sustained inactivation of host erythrocyte APEH is required prior to merozoite invasion and during parasite asexual development. Together, these findings provide evidence for an essential catalytic role for parasite-internalized APEH.

IMPORTANCE Nearly half a million deaths were attributed to malaria in 2017. Protozoan parasites of the genus *Plasmodium* cause disease in humans while replicating asexually within the host's erythrocytes, with *P. falciparum* responsible for most of the mortality. Understanding how *Plasmodium* spp. have adapted to their unique host erythrocyte environment is important for developing malaria control strategies. Here, we demonstrate that *P. falciparum* coopts a host erythrocyte serine hydrolase termed acylpeptide hydrolase. By showing that the parasite requires acylpeptide hydrolase activity for replication, we expand our knowledge of host cell factors that contribute to robust parasite growth.

KEYWORDS *Plasmodium*, acylpeptide hydrolase, erythrocyte, malaria, serine hydrolase

In 2017, an estimated U.S. $3.1 billion was spent on malaria control worldwide. Despite this expenditure, around half a million deaths due to malaria were reported that year (1). *Plasmodium falciparum*, one of the five species that cause human malaria, accounts for the vast majority of these deaths (1). While still unacceptably large, the latest mortality figure represents a substantial improvement on the malaria situation of 15 years ago, which is due in part to the implementation of artemisinin combination therapy (2). Recent reports of reduced efficacy in Southeast Asia have raised concerns that parasites are evolving resistance (or tolerance) to artemisinin-related compounds

Citation Elahi R, Dapper C, Klemba M. 2019. Internalization of erythrocyte acylpeptide hydrolase is required for asexual replication of *Plasmodium falciparum*. mSphere 4:e00077-19. https://doi.org/10.1128/mSphere.00077-19.

Editor Ron Dzikowski, The Hebrew University

Address correspondence to Michael Klemba, klemba@vt.edu.

Received 31 January 2019
Accepted 25 April 2019
Published 8 May 2019

and their partner drugs (3, 4). The discovery and validation of new antimalarial targets are therefore a critical component of a robust antimalarial pipeline, which is needed to safeguard recent advances and to devise strategies for eradication.

Enzymes of the serine hydrolase superfamily encompass a highly diverse range of catalytic activities and have garnered much attention for their roles in many critical metabolic processes in humans (5, 6). Based on annotated sequence homologies, the *P. falciparum* genome encodes over 40 putative members of the serine hydrolase superfamily (7), most of which have not been functionally characterized. Exploration of the roles of uncharacterized serine hydrolases will lead to new insights into essential aspects of parasite metabolism and possibly to new chemotherapeutic targets.

Serine hydrolase-directed activity-based probes (ABPs) have emerged as powerful tools for the functional annotation of serine hydrolases in complex proteomes (5, 8). By enabling competitive activity-based protein profiling (ABPP), ABPs have greatly accelerated the discovery of inhibitors that are highly specific for individual serine hydrolases (5). ABPs containing a fluorophosphonate (FP) warhead provide broad coverage of the serine hydrolase superfamily with negligible off-target activity (9, 10). Reaction of the FP warhead with the active site serine forms a stable covalent adduct. ABPs containing a fluorescent reporter enable a direct quantitative readout of the levels of active serine hydrolases (10).

We have employed a fluorescent FP probe in conjunction with well-characterized serine hydrolase inhibitors to profile the serine hydrolase activities of asexual intraerythrocytic *P. falciparum*. In the course of these studies, we made the surprising discovery that a human host erythrocyte serine hydrolase, acylpeptide hydrolase (APEH; EC 3.4.19.1; also referred to as acylamino acid releasing enzyme and acylaminoacyl-peptidase), is one of the most abundant serine hydrolases in the developing asexual parasite. APEH is a member of the prolyl oligopeptidase (POP) family of serine peptidases (clan SC, family S9C). In mammals, APEH is ubiquitously expressed (11) and has been purified from human erythrocytes as a homotetramer (12, 13). APEH was initially identified as an exopeptidase that catalyzes the hydrolysis of N-terminally acylated amino acids from peptides, yielding an acylamino acid and a shortened peptide with a free N terminus (14, 15). Acetylated and formylated peptides are good substrates for APEH (16, 17). There have also been reports of APEH endopeptidase activity against oxidized proteins (18) and amyloidogenic Aβ peptide (19).

The physiological roles of APEH in mammalian cells are not completely understood. On the basis of the exopeptidase activity of APEH noted above, it has long been hypothesized that APEH participates in the maturation of proteins through the removal of acetylated N-terminal residues (20). Treatment of mouse T cells with a potent and highly selective inhibitor of APEH, termed AA74-1, affected the acetylation status of 25 proteins, lending support for this hypothesis (21). There is some evidence that APEH influences activity of the proteasome (22, 23); however, the mechanistic details of this interaction remain to be elucidated.

Here, we have employed the fluorescent activity-based serine hydrolase probe 6-carboxytetramethylrhodamine–fluorophosphonate (TAMRA-FP), the covalent triazole urea APEH inhibitor AA74-1, and anti-APEH antibodies to explore the properties and physiological role of the parasite-internalized enzyme.

RESULTS

Identification of human APEH in saponin-isolated *P. falciparum*. As a first step toward a proteome-wide functional annotation of serine hydrolase activities in asexual *P. falciparum*, we compared the TAMRA-FP labeling profiles of crude lysates of uninfected erythrocytes and of saponin-isolated parasites (Fig. 1A). Saponin selectively permeabilizes the erythrocyte plasma membrane and the parasitophorous vacuole (PV) membrane of parasite-infected red blood cells; thus, saponin-treated parasites lack soluble erythrocyte and PV proteins (24). Unsurprisingly, there is little overlap between the two profiles, which is consistent with an organism-specific pattern of serine hydrolase expression.

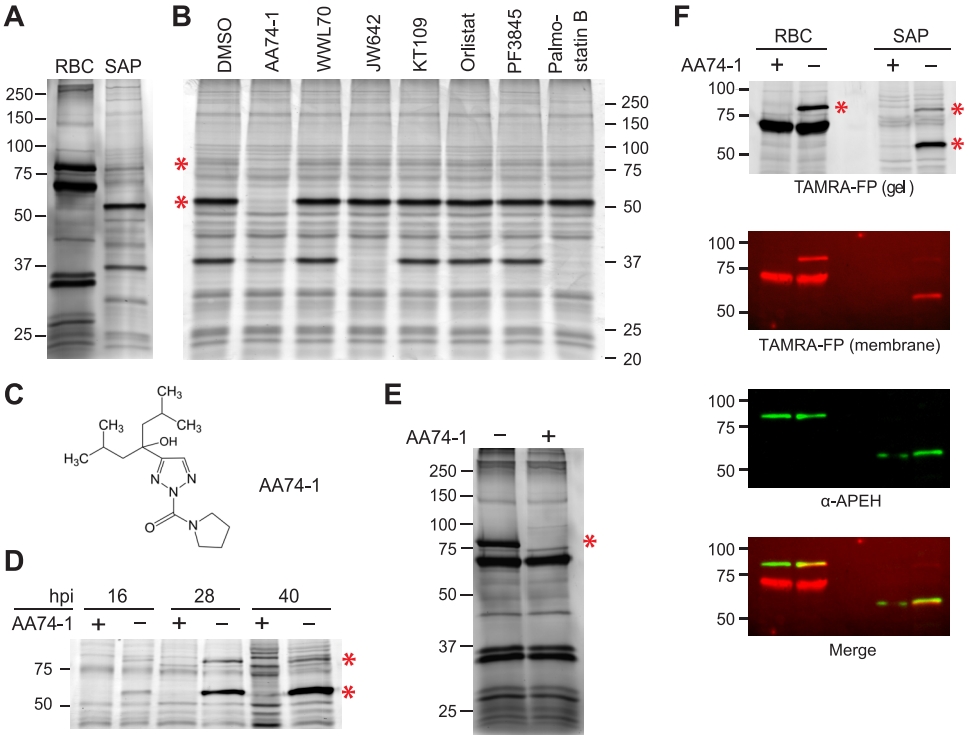

FIG 1 Identification of human APEH in saponin-isolated *P. falciparum*. (A) TAMRA-FP labeling of serine hydrolases in lysates of uninfected human erythrocytes (RBC) and saponin-isolated parasites (SAP). (B) Competitive ABPP using a panel of serine hydrolase inhibitors (1 μM) that target various classes of serine hydrolase (see Table S1) or vehicle (1% DMSO) control. The 80- and 55-kDa species that react quantitatively with AA74-1 are indicated with red asterisks. (C) Structure of the APEH-selective inhibitor AA74-1. (D) Levels of the parasite-internalized 55- and 80-kDa species (red asterisks) throughout the asexual replication cycle. Similar numbers of ring (16 h postinvasion [hpi])-, trophozoite (28 hpi)-, and schizont (40 hpi)-stage parasites were labeled with TAMRA-FP without and with AA74-1 competition. (E) Effect of AA74-1 (1 μM) on TAMRA-FP labeling of serine hydrolases in a lysate of uninfected erythrocytes. The red asterisk indicates an 80-kDa species that is inhibited by AA74-1. (F) Immunodetection of human APEH in lysates of uninfected erythrocytes and saponin-isolated parasites. Lysates were labeled with TAMRA-FP without and with AA74-1 competition, and labeled proteins were detected by in-gel fluorescence scanning ["TAMRA-FP (gel)"]. Proteins were transferred to a nitrocellulose membrane, and TAMRA-FP-labeled species were imaged ["TAMRA-FP (membrane)"]. Because the imaging of TAMRA fluorescence from the nitrocellulose membrane is much less sensitive than in-gel scanning, only the major TAMRA-FP-labeled species are visible. APEH was then detected using an anti-human APEH antibody ("α-APEH"). An overlay of the membrane TAMRA and antibody signals, generated by aligning the molecular markers, is shown in "Merge." TAMRA fluorescence is pseudocolored red, and chemiluminescence is pseudocolored green. The uncropped images are provided in Fig. S2. Sizes of molecular markers are indicated in kDa.

To gain insight into the functionality of *P. falciparum* serine hydrolases, competitive activity-based probe profiling (referred to as competitive ABPP) was conducted. Crude lysates of saponin-isolated parasites were incubated with covalent inhibitors of diverse human serine hydrolases or vehicle (1% DMSO) prior to TAMRA-FP labeling (Fig. 1B; structures of inhibitors and their known targets are provided in Table S1 in the supplemental material). We were intrigued to find that AA74-1, a triazole urea inhibitor (Fig. 1C) that is highly selective for human APEH (21), completely blocked TAMRA-FP labeling of a major ~55-kDa species and a minor ~80-kDa species in parasite lysate (Fig. 1B). In contrast, lipase or fatty acid amide hydrolase inhibitors did not compete with labeling of the 55- or 80-kDa species (Fig. 1B). Both of these species are present in ring-stage parasites, and the abundance of the 55-kDa species increases throughout the asexual replication cycle (Fig. 1D). Treatment of erythrocyte lysate with the same inhibitor panel revealed that AA74-1, but not lipase or fatty acid amide hydrolase inhibitors, blocked TAMRA-FP labeling of an ~80-kDa species in a highly selective manner (Fig. 1E; Fig. S1). The estimated molecular mass of this species is consistent with a predicted molecular mass of 81.2 kDa for human APEH (25).

The above findings suggest two possible interpretations: (i) *P. falciparum* expresses an endogenous protein with activity similar to that of human APEH or (ii) the parasite internalizes the erythrocyte enzyme. To distinguish between these possibilities, we asked whether parasite-internalized APEH is recognized by an affinity-purified anti-human APEH antibody (Fig. 1F). Parasite and erythrocyte lysates were first analyzed by competitive ABPP with and without AA74-1 to identify APEH. After in-gel fluorescence scanning of TAMRA-FP-labeled species, the proteins were transferred to nitrocellulose, and membrane-associated TAMRA fluorescence was imaged. APEH was then detected by chemiluminescent immunoblotting (Fig. 1F). When the membrane TAMRA and chemiluminescence images were merged by aligning the molecular markers, overlap of signal was observed for the erythrocyte 80-kDa species and the parasite-internalized 55-kDa species. These findings strongly suggest that *P. falciparum* internalizes host cell APEH, which then appears to undergo a proteolytic event to reduce the size of the active site-containing segment from 80 to 55 kDa. The minor ~80-kDa species in parasite lysate that is inhibited by AA74-1 likely represents full-length, uncleaved APEH. Here, these two species will be collectively referred to as "parasite-internalized APEH."

Validation of AA74-1 as a potent and selective inhibitor of parasite-internalized APEH. Before using AA74-1 to probe the importance of internalized APEH for intraerythrocytic parasite development, we evaluated its potency and selectivity in cell lysates. The 50% inhibitory concentration (IC_{50}) values for AA74-1 inhibition of erythrocyte and parasite-internalized APEH were determined by competitive ABPP (Fig. 2A and B). Mean IC_{50} values from three independent replicates were 7.9 ± 1.8 nM for the parasite 55-kDa species and 7.4 ± 2.4 nM for the erythrocyte 80-kDa species, which are not significantly different (two-tailed Student's *t* test, *P* value = 0.78). These values are very close to the 11 nM IC_{50} value reported for AA74-1 inhibition of APEH in a human cell line using a similar competitive ABPP assay (21). The parasite 80-kDa species appeared to have a comparable IC_{50} value (Fig. 2A), but its lower abundance made it difficult to reliably quantify this species.

To assess the selectivity of AA74-1 for APEH in saponin-isolated parasite lysate, the fluorescence profiles of the lanes corresponding to 135 and 405 nM AA74-1 in Fig. 2A were compared to that of the vehicle (DMSO) control (Fig. 2C). At both concentrations, the 80- and 55-kDa APEH species were effectively inhibited (Fig. 2C, red asterisks). A 37-kDa species was partially inhibited at both concentrations. In separate studies, we have identified this species as the "prodrug activation and resistance esterase" (R. Elahi, C. Dapper, and M. Klemba, unpublished data), a serine hydrolase that is not essential for asexual replication of *P. falciparum* (55). We conclude that concentrations of AA74-1 below ~400 nM are highly selective for the 55- and 80-kDa species of APEH in saponin-isolated parasite lysate *in vitro*.

The antimalarial potency of AA74-1 is enhanced over two replication cycles. To determine whether internalized APEH is required for efficient parasite replication, we examined the effect of AA74-1 on the development of a synchronized ring-stage *P. falciparum* culture. Parasite replication was assessed by measuring the fluorescence of the DNA-binding dye SYBR green I after 48 h (the time required for one complete cycle of the 3D7 line is ~42 h). AA74-1 was a relatively poor inhibitor of parasite growth, with incomplete inhibition of parasite replication at 10 μM and an estimated 50% effective concentration (EC_{50}) greater than 1 μM (Fig. 3A; Table 1). Interestingly, however, when parasites were seeded at a lower density and allowed to proceed through two replication cycles (96 h), the efficacy of AA74-1 increased by over 10-fold, exhibiting a mean EC_{50} value of 96 ± 38 nM over three biological replicates (Fig. 3A; Table 1). Near-complete inhibition of parasite replication on the second cycle was observed at an AA74-1 concentration of 310 nM, a value that is highly selective for APEH in saponin-isolated parasite lysate (Fig. 2B). In contrast to these results, parallel experiments with chloroquine yielded 48- and 96-h EC_{50} values that were not significantly different (Table 1; two-tailed Student's *t* test, *P* value = 0.93).

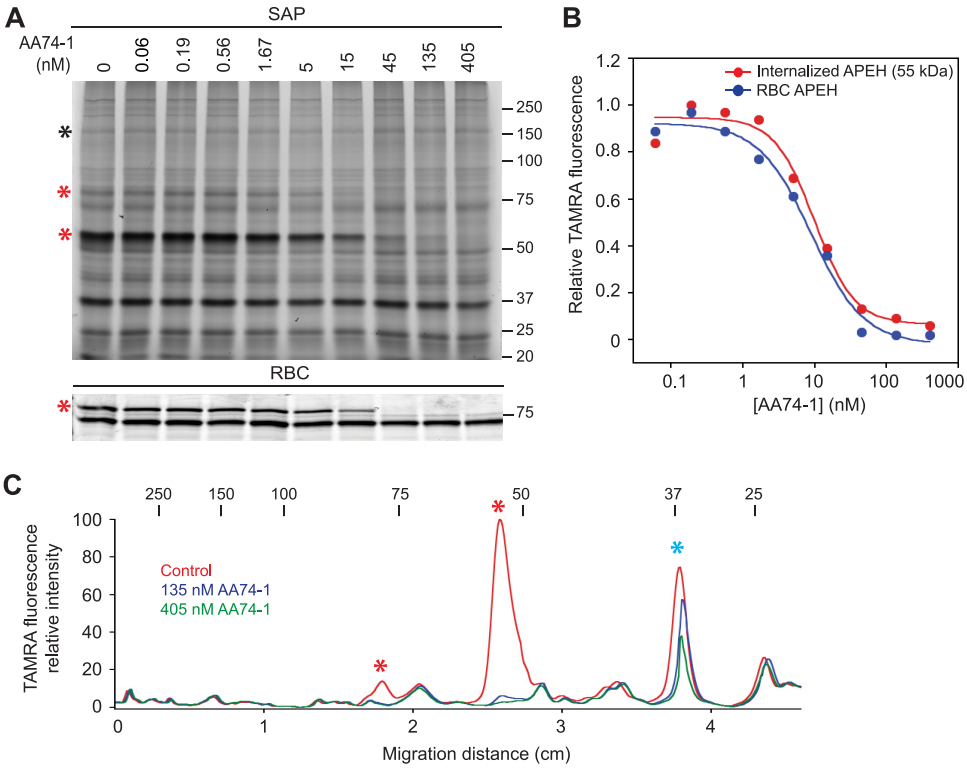

FIG 2 Potency and selectivity of AA74-1 in lysates of saponin-isolated parasites and uninfected erythrocytes. (A) Competitive ABPP with AA74-1 over a concentration range of 0.06 to 405 nM. (Upper panel) Saponin-isolated parasites (SAP). The 55- and 80-kDa APEH species are indicated with red asterisks. The species used for APEH peak volume normalization (see Materials and Methods) is indicated with a black asterisk. (Lower panel) Uninfected erythrocytes (RBC). APEH is indicated with a red asterisk. See Fig. S3 for the full gel image and the species used for peak volume normalization. (B) Plot of normalized APEH peak volume, expressed as a fraction of the control ("0 nM," 1% DMSO), versus AA74-1 concentration. Data are from the gel images in panel A, which represent one of three biological replicates. Points were fitted to a four-parameter sigmoidal curve. (C) Selectivity of AA74-1 in lysates of saponin-isolated parasites. TAMRA fluorescence profiles were generated for lanes in panel A corresponding to 0, 135, and 405 nM AA74-1. The 55- and 80-kDa internalized APEH species are indicated with red asterisks. Prodrug activation and resistance esterase is indicated with a blue asterisk. For panels A and C, the molecular masses of markers are indicated in kDa.

Dramatic enhancement of antimalarial potency during a second replication cycle is a hallmark of compounds that target the *P. falciparum* apicoplast (27, 28) and is referred to as "delayed death." An apicoplast-based delayed death response can be reversed by supplementation of parasite culture medium with 200 μM isopentenyl pyrophosphate (IPP), which is the sole product of apicoplast metabolism that is required during the asexual growth cycle (27). To determine whether the enhanced potency of AA74-1 might be due to inhibition of an apicoplast enzyme, we conducted 96-h growth assays in the presence and absence of 200 μM IPP. As a positive control for delayed death, parallel experiments were performed with clindamycin, an antibiotic that targets the apicoplast. Clindamycin has been shown to exhibit a profound delayed death response, which can be rescued by IPP supplementation (27, 28). While clindamycin toxicity was dramatically attenuated in the presence of IPP (Fig. 3B; Table 1), the potency of AA74-1 was unaffected (Fig. 3A; Table 1). These results strongly suggest that AA74-1 does not target an apicoplast enzyme and indicate that an alternate mechanism lies behind the enhancement of AA74-1 potency during the second replication cycle.

To determine whether the duration of parasite exposure to AA74-1 during the first replication cycle influences the enhanced potency observed during the second, we compared the effects of adding AA74-1 at the start of cycle 1 (i.e., ring stage) or at the end (i.e., schizont stage; a schematic diagram of the experimental design is shown in Fig. 3C). As expected, there was a pronounced leftward shift in the concentration-

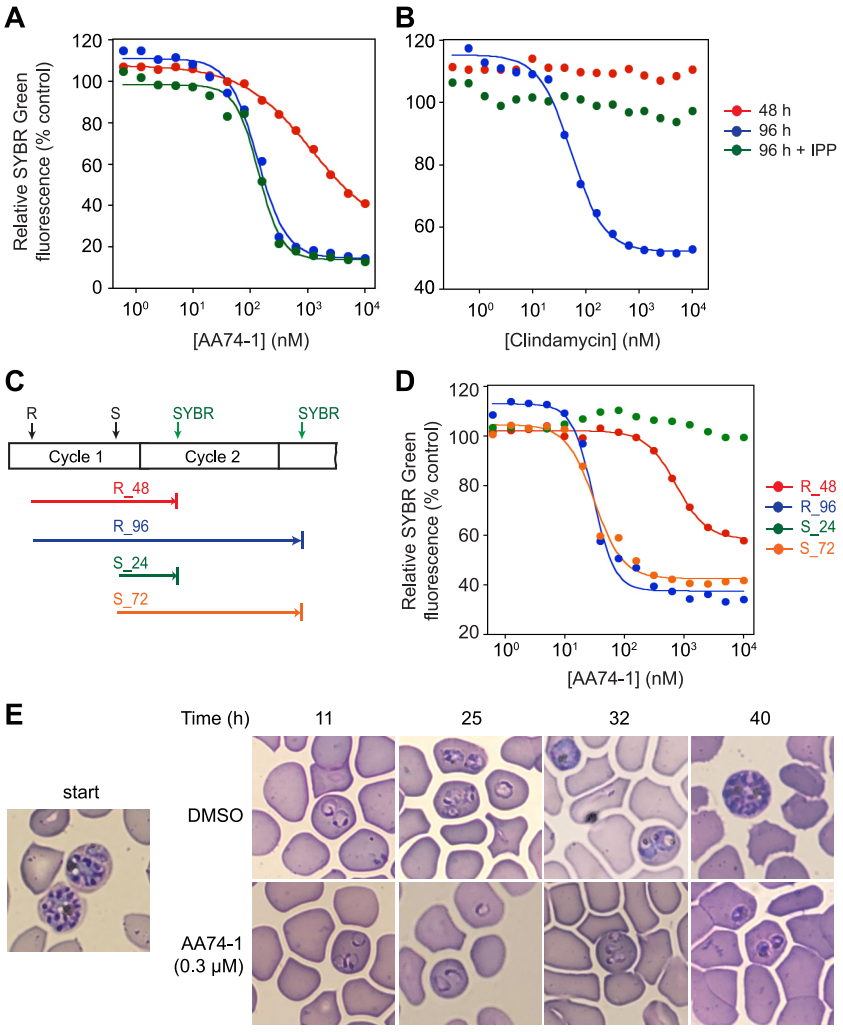

FIG 3 Effects of AA74-1 on parasite replication. (A and B) Concentration-response plots for parasites cultured in the presence of AA74-1 (A) or clindamycin (B) for 48 h (red circles), 96 h (blue circles), or 96 h in the presence of 200 μM IPP (green circles). At the indicated time points, parasite DNA was quantified using a SYBR green I assay. Data are expressed as a percentage of the fluorescence value for the vehicle (DMSO) control. (C) Schematic diagram of the concentration-response experiment in panel D. Addition of AA74-1 is indicated with black arrows and occurred at either ring (R) or schizont (S) stage. SYBR green I assays of parasite cultures were conducted after completion of cycle 1 and cycle 2 (green arrows). The colored arrows indicate incubation periods for ring cultures (48 and 96 h, abbreviated R_48 and R_96, respectively) and schizont cultures (24 and 72 h, abbreviated S_24 and S_72, respectively). (D) Concentration-response curves for AA74-1 treatment initiated at ring or schizont stages of asexual development. Plot line colors correspond to those of the arrows in panel C. In panels A, B, and D, inhibition curves were generated by nonlinear regression fits to a four-parameter sigmoidal curve. The lower baselines are nonzero due to background fluorescence. (E) Stage specificity of AA74-1 toxicity. Schizont-stage parasites were treated with 0.3 μM AA74-1 or DMSO vehicle. Typical sections of Giemsa-stained smears at the start of the experiment ("start") and at various times in hours after initiation of treatment are shown.

response curve during the second cycle when AA74-1 was added at the ring stage (compare ring 48- and 96-h data sets [Fig. 3D; Table 2]). When AA74-1 was added at the schizont stage, there was no effect on SYBR green I signal after 24 h. Strikingly, the concentration-response curve over the second cycle yielded EC_{50} values that were essentially identical to those when AA74-1 was added at ring stage (compare ring 96-h and schizont 72-h data sets [Fig. 3D; Table 2]; two-tailed Student's *t* test, *P* value = 0.74). These results reveal that AA74-1 does not induce a delayed death response; rather, they suggest that for AA74-1 to exert parasiticidal activity, host cells must be exposed to the inhibitor prior to merozoite invasion. Parallel experiments with chloroquine yielded

TABLE 1 Effects of incubation time and IPP on EC_{50} values from ring-initiated *P. falciparum* growth inhibition assays[a]

	Mean EC_{50} (nM) ± SD for incubation time and IPP presence		
		96 h	
Compound	48 h	−IPP	+IPP
AA74-1	>1,000	96 ± 38	94 ± 39
Clindamycin	>10,000	37 ± 24	>10,000
Chloroquine	9.0 ± 2.4	8.5 ± 2.0	ND

[a]Values are means from three biological replicates. ND, not determined.

highly similar EC_{50} values at all incubation times longer than 24 h (Table 2). To confirm that AA74-1 effectively blocks host cell APEH over the duration of the schizont-initiated growth experiment, uninfected erythrocytes were treated with 100 nM AA74-1 or DMSO vehicle; sampled at 4, 24, and 72 h; and assayed for APEH activity after inhibitor washout. Complete inhibition of erythrocyte APEH was observed at all time points (Fig. S4).

Finally, we assessed the stage specificity of AA74-1 toxicity by treating synchronized late-stage schizonts with 300 nM AA74-1 and following parasite development by Giemsa-stained smears. AA74-1 did not block merozoite egress or invasion, as indicated by the presence of ring-stage parasites 11 h after adding AA74-1 (Fig. 3E). After 40 h, the control culture had developed into mature schizonts, whereas growth of AA74-1-treated parasites had halted at the early trophozoite stage (Fig. 3E).

Parasite-internalized APEH, but not erythrocyte APEH, is recalcitrant to AA74-1 inhibition in intact cells. Seeking an explanation for the enhanced potency of AA74-1 during the second replication cycle, we asked whether AA74-1 is an effective inhibitor of parasite-internalized APEH in intact parasitized erythrocytes. Because AA74-1 covalently modifies the active site serine of APEH (21), the inhibitor can be added to parasite cultures for a defined period of time and the extent of APEH inhibition *in vivo* can be assessed by TAMRA-FP labeling following inhibitor washout and saponin isolation of parasites. We determined the amount of residual internalized APEH activity following a 4-h treatment of cultured trophozoite-stage parasites with 0.1, 1, or 10 μM AA74-1. A 4-h treatment window was selected in order to minimize the potentially confounding effects of toxicity at the higher AA74-1 concentrations (Fig. 3A). Surprisingly, parasite-internalized APEH was not effectively inhibited by exogenous AA74-1 concentrations up to 10 μM (Fig. 4A). A parallel experiment with uninfected erythrocytes demonstrated robust inhibition of APEH at all exogenous AA74-1 concentrations (Fig. 4A). These results indicate that the inhibitor is able to diffuse across the erythrocyte plasma membrane but is unable to inhibit APEH within the parasite.

To further explore this phenomenon, we conducted an experiment to determine whether there was something distinctive about *P. falciparum*-infected erythrocytes that prevented accumulation of AA74-1. Trophozoite-stage parasites were treated for 4 h with 100 nM exogenous AA74-1, washed extensively, and purified on a magnetic column to >90% parasitemia (this material is referred to as "pRBCs"). We then fractionated the pRBCs with saponin, yielding a supernatant containing host erythrocyte APEH and a pellet containing parasite-internalized APEH. A schematic of the experi-

TABLE 2 EC_{50} values from *P. falciparum* growth inhibition assays initiated with ring- or schizont-stage parasites[a]

	Mean EC_{50} (nM) ± SD			
Compound	Schizont, 24 h	Ring, 48 h	Schizont, 72 h	Ring, 96 h
AA74-1	>10,000	>1,000	47 ± 30	40 ± 10
Chloroquine	>250	29 ± 9	35 ± 10	28 ± 4

[a]For each data column, the stage of initiation and time of incubation are indicated. Values are from three biological replicates.

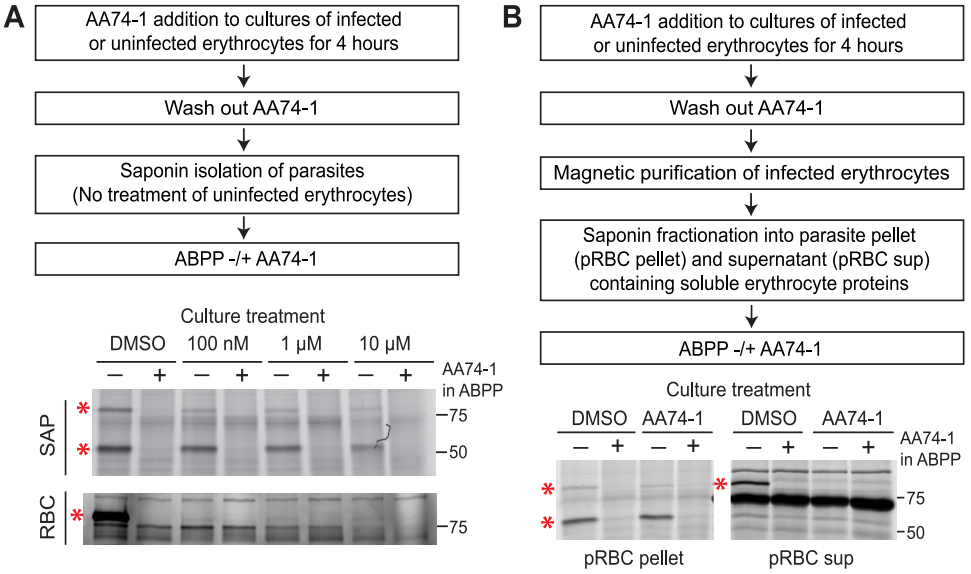

FIG 4 Analysis of AA74-1 inhibition of APEH in intact cells. (A) Characterization of APEH inhibition upon AA74-1 treatment of cultured *P. falciparum*-infected or uninfected erythrocytes. (Upper panels) Flow diagram of the experimental approach. (Lower panels) TAMRA-FP labeling of active APEH in saponin-isolated parasites (SAP) and uninfected erythrocytes (RBC). (B) Characterization of APEH inhibition by AA74-1 in the infected erythrocyte cytosol and in saponin-isolated parasites. (Upper panels) Flow diagram of the experimental approach. (Lower panels) TAMRA-FP labeling of active APEH in the saponin-isolated parasite pellet (pRBC pellet) or the saponin supernatant containing soluble host erythrocyte proteins (pRBC sup) obtained from highly purified infected erythrocytes following treatment with 100 nM AA74-1. In both panel A and panel B, ABPP was conducted with and without 1 μM AA74-1 ("AA74-1 in ABPP") to identify APEH species (red asterisks). One biological replicate is shown out of two that yielded similar results. Molecular masses of markers are indicated in kDa.

mental design is shown in Fig. 4B. Once again, we observed inhibition of erythrocyte APEH but not parasite-internalized APEH (Fig. 4B).

Parasite-internalized APEH is active and is inhibited by AA74-1 at acidic pH. The most likely scenario for internalization of host cell APEH is through the endocytosis of large quantities of erythrocyte cytosol and delivery to the food vacuole (see Discussion). The lumen of the food vacuole is acidic with a pH of ~5.5 (29, 30). To determine whether APEH could have a catalytic role at this pH, we asked whether TAMRA-FP modifies the active site serine of APEH at pH 5.5. While APEH was labeled with TAMRA-FP at pH 5.5 (Fig. 5), the extent of labeling was lower at pH 5.5 than at 7.4, which suggests a lower reaction rate at the acidic pH value. We also found that AA74-1 is capable of inhibiting APEH at pH 5.5 *in vitro* (Fig. 5); thus, an acidic pH does not by itself explain the recalcitrance of parasite-internalized APEH to AA74-1 inhibition in intact parasitized erythrocytes.

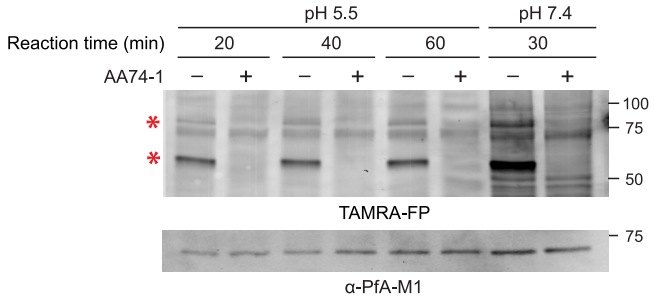

FIG 5 APEH activity and inhibition by AA74-1 at acidic pH. (Upper panel) ABPP of saponin-isolated parasite lysates at pH 5.5 and 7.4. Times of TAMRA-FP labeling reactions are indicated. Each reaction was conducted with and without 1 μM AA74-1 to identify APEH. (Lower panel) Anti-PfA-M1 immunoblot assay to indicate relative loading levels. Red asterisks indicate the 55- and 80-kDa internalized APEH species. Molecular masses of markers are indicated in kDa.

DISCUSSION

We present evidence that *P. falciparum* internalizes and accumulates erythrocyte APEH during its growth in the host cell. There are several reported examples of *P. falciparum* importing host cell proteins for metabolic purposes, including superoxide dismutase (31), δ-aminolevulinate dehydratase (26), and peroxiredoxin 2 (32). APEH is the first example to our knowledge of a hydrolytic host enzyme accumulating in the parasite.

The most likely route for internalization of erythrocyte APEH is through the cytostomal endocytic pathway that is responsible for the uptake and delivery to the food vacuole of large quantities of erythrocyte cytosol (33–35). Up to 75% of erythrocyte hemoglobin, the dominant constituent of erythrocyte cytosol, is internalized through this pathway (36). Because cytostomal endocytosis is thought to be a nonspecific process, APEH would presumably be delivered to the food vacuole along with hemoglobin and other soluble erythrocyte proteins. This model for APEH internalization is consistent with the observed proteolysis of parasite APEH to a 55-kDa species, which may be mediated by vacuolar aspartic and cysteine endopeptidases (37). Our findings are consistent with those of several previous studies demonstrating that APEH is highly resistant to proteolytic degradation and that endoproteases such as trypsin, chymotrypsin, and elastase clip full-length, 80-kDa APEH into ~55-kDa and ~25-kDa fragments *in vitro* (38–41). Interestingly, these studies have established that this proteolytic treatment neither disrupts the homotetrameric structure of APEH nor reduces its activity (38, 39), thus providing a plausible explanation for the stability of APEH in the proteolytic environment of the food vacuole. The shift in size of APEH in saponin-isolated parasite lysates indicates that it does not originate from contamination by host erythrocyte cytosol or from interaction with the outer leaflet of the parasite plasma membrane. We have tried to confirm a food vacuole location for APEH through indirect immunofluorescence using anti-APEH antibodies; however, although we have tested a wide range of fixation conditions and numerous antibodies, we have not found conditions that are suitable for detection of APEH in infected erythrocytes.

To investigate the possibility of a physiological role for internalized APEH, we employed the APEH-selective inhibitor AA74-1 that was discovered in a library of triazole urea compounds by Cravatt and colleagues (21). The exquisite selectivity of this covalent inhibitor for APEH has been demonstrated *in vitro* using mouse T cell lysates and *in situ* using cultured T cells (21). Furthermore, upon treatment of mouse T cells with AA74-1, the N-terminal acetylation state of ~25 endogenous proteins was altered, which indicates that AA74-1 is able to engage its target *in situ* (21). Thus, we considered AA74-1 to be an appropriate tool for the interrogation of APEH function in *P. falciparum*. To validate the use of AA74-1 in the context of *P. falciparum*-infected erythrocytes, we demonstrated by competitive ABPP that the inhibitor is highly selective for parasite-internalized APEH in lysates of saponin-isolated parasites at concentrations below ~400 nM. It is also selective for APEH in uninfected erythrocytes.

When AA74-1 was added to synchronized ring-stage parasites, inhibition of growth over the first replication cycle required concentrations that were much higher than those needed to inhibit APEH *in vitro*. However, a dramatic enhancement of potency was observed if the growth inhibition experiment was continued for a second replication cycle, i.e., 96 h. Notably, the EC_{50} for growth inhibition after the second cycle was only 12-fold higher than the IC_{50} observed for inhibition of APEH in competitive ABPP. Furthermore, the AA74-1 concentrations that yielded efficient inhibition of growth replication were within the concentration range found to be highly selective (i.e., below 400 nM). Taken together, the evidence strongly suggests that the growth defect observed during the second cycle is due to the selective targeting of APEH.

Enhancement of drug potency during a second replication cycle is commonly observed with inhibitors that target the parasite apicoplast (42). Our experiments with IPP supplementation, however, revealed that internalized APEH is not acting in the context of the apicoplast, nor is AA74-1 cross-inhibiting an apicoplast enzyme. Further-

more, we found that addition of AA74-1 late in the developmental cycle was sufficient to promote high-potency parasiticidal activity during the ensuing cycle.

Analysis of AA74-1 inhibition of APEH within intact cells yielded a critical insight that may explain the peculiar antimalarial characteristics of AA74-1 described above. When added to culture medium, AA74-1 effectively inhibited the host erythrocyte pool of APEH but not the two parasite-internalized APEH species. The reason for the recalcitrance of parasite-internalized APEH is not entirely clear. If APEH resides in the food vacuole, it will experience an acidic pH; however, we have demonstrated that the 55-kDa APEH species reacts with AA74-1 at pH 5.5 *in vitro*. It is possible that AA74-1 is not able to access the lumen of the food vacuole or that it is inactivated inside the parasite by a hydrolytic enzyme. Parasite-internalized APEH is present in ring-stage parasites, an observation that is consistent with prior reports of cytostomal endocytosis occurring during early in asexual development (35, 43). We propose that the second-cycle enhancement of AA74-1 potency described above occurs because the erythrocyte APEH pool is inhibited prior to merozoite invasion. Thus, parasites internalize inactive APEH from the onset of asexual development and do not accumulate an AA74-1-recalcitrant pool of the enzyme.

Our findings lead us to the intriguing idea that *P. falciparum* has adapted to use internalized APEH for a crucial metabolic function. The most apparent role for APEH, if as expected it resides in the food vacuole, is in catalyzing the hydrolysis of acetylated amino acids from the N termini of peptides generated through the catabolism of endocytosed erythrocyte proteins. This role would be consistent with the observed cytotoxicity of AA74-1 at the early trophozoite stage, a point in asexual development at which the endocytosis and degradation of erythrocyte cytosol accelerate (36). The two most abundant cytosolic proteins in the erythrocyte are hemoglobin (composed of α- and β-globin in the adult) and carbonic anhydrase-1, which are present at 97% and 1% of total protein, respectively (44). While α- and β-globin have not traditionally been thought to have acetylated N termini, a proteome-wide analysis of erythrocyte proteins that explicitly addressed the acetylation status of N termini found that about 20% of the dominant species of both α- and β-globin are N acetylated (45). Carbonic anhydrase-1 is known to possess an acetylated N terminus (46). Furthermore, proteomic studies have identified over 1,500 soluble erythrocyte proteins (47, 48), around 53% of which are N terminally acetylated (45). Given the large quantities of erythrocyte cytosol that are digested in the food vacuole, a mechanism is likely needed for efficient removal of N-acetylated amino acids from peptides generated by endoproteolytic hydrolysis, as N-blocked peptides are expected to be poor substrates for the vacuolar exopeptidase dipeptidyl aminopeptidase 1 and the M1- and M24-family aminopeptidases *P. falciparum* A-M1 (PfA-M1) and PfAPP (49, 50). Although the pH optimum of human erythrocyte APEH is reported to be close to neutral pH (13, 51), TAMRA-FP labeling at pH 5.5 strongly suggests that parasite-internalized APEH retains catalytic activity, albeit diminished, at the acidic pH of the food vacuole. The cointernalization of host cell APEH could provide the parasite with an elegant solution for the need to catabolize N-acetylated peptides.

MATERIALS AND METHODS

Reagents. The TAMRA-fluorophosphonate activity-based probe was obtained from ThermoFisher. *N*-(*trans*-epoxysuccinyl)-L-leucine-4-guanidinobutylamide (E-64), AA74-1, clindamycin, chloroquine, and isopentenyl pyrophosphate trilithium salt were purchased from Sigma. Pepstatin A was purchased from MP Biomedicals.

Parasite culture. *P. falciparum* 3D7 was cultured in human O^+ erythrocytes (Interstate Blood Bank, Memphis, TN) at 2% hematocrit in RPMI 1640 medium supplemented with 27 mM sodium bicarbonate, 11 mM glucose, 0.37 mM hypoxanthine, 10 μg/ml gentamicin, and 5 g/liter AlbuMAX I (Invitrogen). Unless otherwise indicated, cultures were incubated at 37°C in a 5% CO_2 incubator. Cultures were synchronized by treatment with 5% (wt/vol) sorbitol (52).

Preparation of parasite lysate. Synchronized parasites were separated from soluble erythrocyte and parasitophorous vacuole proteins by treatment with 0.03% (wt/vol) saponin in cold Dulbecco's phosphate-buffered saline (PBS; pH 7.4) for 10 min on ice. Unless indicated otherwise, parasites were harvested at 32 to 40 h postinvasion (hpi). Saponin-isolated parasites were recovered by centrifugation at 1,940 $\times$ *g* at 4°C for 10 min and were washed three times with cold PBS. The yield of parasites was

determined by counting on a hemocytometer. Parasites were suspended to a density of 5×10^8 parasites/ml in cold PBS containing the protease inhibitors pepstatin A (5 μM) and E-64 (10 μM). The parasite suspension was subjected to three rounds of sonication at 30% power for 10 s. After centrifugation at 17,000 $\times$ *g* to pellet cellular debris, aliquots of clarified lysates were snap-frozen in liquid N_2 and stored at −80°C.

Preparation of uninfected erythrocyte lysate. Uninfected erythrocytes were washed three times in cold PBS, counted on a hemocytometer, and resuspended in cold PBS containing 5 μM pepstatin A and 10 μM E-64 to a density of 5×10^8 cells/ml. Lysates of resuspended erythrocytes were prepared and stored as described above for saponin-isolate parasites.

Activity-based protein profiling. TAMRA-FP labeling reactions were conducted with 19.8 μl of parasite or erythrocyte lysate, which corresponds to ~10^7 cells/reaction mixture. To start the reaction, 0.2 μl of 100 μM TAMRA-FP was added, giving a final concentration of 1 μM. Reaction mixtures were incubated at 30°C for 30 min and then stopped by the addition of 1 volume of 2× reducing SDS-PAGE loading buffer and incubation at 95°C for 5 min. For competitive ABPP experiments, inhibitor or vehicle (DMSO) was added and reaction mixtures were incubated for 20 min at 30°C prior to the addition of TAMRA-FP. Labeled proteins were resolved on 8.5% or 10% reducing SDS-polyacrylamide gels. In-gel TAMRA fluorescence was recorded on a Typhoon Trio flatbed scanner (GE Healthcare Life Sciences, Piscataway, NJ). Fluorescence profiles and peak volumes of labeled proteins were obtained using ImageQuant TL v2005 (GE Healthcare Life Sciences, Piscataway, NJ). For calculation of AA74-1 IC_{50} values, the peak volume for the 55-kDa APEH species in saponin-isolated parasites was normalized to that of an ~160-kDa species (Fig. 2A, black asterisk) that was not inhibited by AA74-1 at any concentration. Normalization of erythrocyte APEH peak volumes was conducted in a similar manner (see Fig. S3 in the supplemental material). IC_{50} values were calculated by nonlinear regression fitting of the data to a four-parameter sigmoidal curve using Kaleidagraph 4.5 (Synergy Software, Reading, PA).

Identification of APEH by immunoblotting. Competitive ABPP on crude lysates from ~10^7 saponin-isolated parasites or uninfected erythrocytes was performed as described above. Following in-gel fluorescence scanning, proteins were transferred to a nitrocellulose membrane and TAMRA fluorescence was imaged with a G:Box ChemiXX6 imager (Syngene, Frederick, MD). The membrane was then blocked with 2% bovine serum albumin in Tris-buffered saline containing 0.1% Tween 20 (TBST/BSA) for 1 h at room temperature, incubated with primary antibody diluted in TBST/BSA for 1 h, and then incubated with horseradish peroxidase-conjugated anti-rabbit secondary antibody (1:10,000; GE Healthcare Life Sciences, Piscataway, NJ) for 1 h. The primary antibody used was affinity-purified anti-APEH rabbit polyclonal antibody (IgG) raised against an APEH fragment consisting of amino acids 381 to 732 (product number 14758-1-AP; Proteintech, Rosemont, IL; 0.26 μg/ml). Chemiluminescent signal was developed with ECL Plus (GE Healthcare life Sciences, Piscataway, NJ) and detected using a G:Box ChemiXX6 imager. Image alignment (using molecular markers) and contrast adjustment were accomplished with Adobe Photoshop CS2 (Adobe, Inc., San Jose, CA).

***P. falciparum* growth inhibition assays.** Synchronized ring-stage cultures were seeded at 3% parasitemia (48-h assay) or 0.6% parasitemia (96-h assay) and 1% hematocrit in a 96-well flat-bottom plate. Inhibitors were added from 1,000× stock solutions in DMSO to generate 2-fold concentration series of AA74-1 (0.61 nM to 10 μM), chloroquine (1.9 to 250 nM), or clindamycin (0.3 nM to 10 μM). After 48 or 96 h of incubation at 37°C under reduced-oxygen conditions (5% O_2, 5% CO_2, and 90% N_2), parasite growth was determined using a SYBR green I DNA quantitation assay as previously described (53). Values from samples containing 0.1% DMSO were used to calculate relative SYBR green I fluorescence. Each assay was performed with two technical replicates, which were averaged to generate a single biological replicate. EC_{50} values were calculated by nonlinear regression fitting of the data to a four-parameter sigmoidal curve using Kaleidagraph 4.5 (Synergy Software, Reading, PA). For experiments with 200 μM IPP supplementation, single technical replicates were conducted for each biological replicate.

To compare the effects of AA74-1 addition at ring and schizont stages, the following modifications were made. An aliquot of a synchronous ring-stage culture was used to set up 48- and 96-h assays as described above. Another aliquot of the culture was allowed to progress to the schizont stage, at which point schizonts were separated from any ring-stage parasites by enrichment on a magnetically activated cell sorting (MACS) magnetic LD column (Miltenyi Biotech, Gaithersburg, MD) according to the manufacturer's instructions. These schizonts were then used to inoculate cultures for 24- and 72-h growth assays. At the indicated time points, SYBR green I assays were conducted. A schematic of the experimental design is provided in Fig. 3C. To assess the extent of host cell APEH inhibition over an extended incubation period, 100 nM AA74-1 or DMSO vehicle was added to uninfected erythrocytes. Cultures were sampled at 4, 24, and 72 h and washed four times in cold RPMI to remove AA74-1. Lysates were prepared as described under "Preparation of uninfected erythrocyte lysate," and APEH activity was assessed with TAMRA-FP.

AA74-1 stage specificity. Synchronized late-stage schizont parasites were cultured in 200-μl volumes in 96-well plates in the presence of 0.3 μM AA74-1 or 0.1% DMSO over a period of 40 h. Parasite development was monitored by making Giemsa-stained thin smears at 11, 25, 32, and 40 h after initiation of treatment.

AA74-1 inhibition of APEH in intact cells. Trophozoite-stage parasites (30 to 38 hpi) or uninfected erythrocytes were incubated in culture medium supplemented with AA74-1 (100 nM, 1 μM, or 10 μM) or with 0.1% DMSO for 4 h at 37°C under reduced-oxygen conditions with gentle mixing on an orbital rotator. Cultures were washed four times in cold RPMI to remove exogenous AA74-1. Parasites were then isolated with saponin as described above. Saponin-isolated parasites and uninfected erythrocytes were

counted with a hemocytometer, resuspended in cold PBS at a cell density of 5×10^8 per ml, and stored at −80°C. Samples were assayed directly by competitive ABPP.

To investigate the inhibition of APEH in the host and parasite compartments of infected erythrocytes, a synchronized trophozoite culture was treated with AA74-1 (100 nM) or with 0.1% DMSO for 4 h at 37°C under reduced-oxygen conditions. The culture was washed four times in cold RPMI to remove AA74-1 and then resuspended in RPMI medium. Parasitized erythrocytes were purified from the culture on a MACS magnetic LD column. Enriched parasitized RBCs (pRBCs) were subjected to saponin treatment as described under "Preparation of parasite lysate." Saponin-isolated parasites (pRBC pellet) and the supernatant containing soluble host erythrocyte proteins (pRBC sup) were collected and stored at −80°C. Samples were used directly for competitive ABPP.

Activity and inhibition of APEH at acidic pH. Saponin-isolated parasites were split into two aliquots and resuspended to a density of 5×10^8 parasites/ml in either PBS (pH 7.4) or 100 mM sodium 2-(*N*-morpholino)ethanesulfonate (MES) (pH 5.5), both of which included 5 μM pepstatin A and 10 μM E-64. Crude lysates were prepared as described under "Preparation of parasite lysate." APEH activity and inhibition by AA74-1 were analyzed as described under "Activity-based protein profiling," with the modification that TAMRA-FP incubation times up to 60 min were employed for reactions conducted at pH 5.5. After fluorescence scanning, proteins were immediately transferred to a nitrocellulose membrane, and relative loading levels were assessed by immunoblotting using affinity-purified anti-PfA-M1 (0.13 μg/ml [54]) and horseradish peroxidase-conjugated anti-rabbit secondary antibody (1:10,000).

SUPPLEMENTAL MATERIAL

Supplemental material for this article may be found at https://doi.org/10.1128/mSphere.00077-19.

FIG S1, TIF file, 2 MB.
FIG S2, TIF file, 2.8 MB.
FIG S3, TIF file, 2 MB.
FIG S4, TIF file, 1.9 MB.
TABLE S1, DOCX file, 0.5 MB.

ACKNOWLEDGMENTS

This work was supported by National Institute of Allergy and Infectious Diseases grant AI133136. The funding agency had no role in study design, data collection and interpretation, or the decision to submit the work for publication.

R.E. and M.K. designed the experiments, R.E. and C.D. conducted the experiments, and R.E. and M.K. prepared the manuscript.

REFERENCES

1. World Health Organization. 2018. World malaria report 2018. World Health Organization, Geneva, Switzerland.
2. World Health Organization. 2013. World malaria report 2013. World Health Organization, Geneva, Switzerland.
3. Dondorp AM, Smithuis FM, Woodrow C, Seidlein LV. 2017. How to contain artemisinin- and multidrug-resistant falciparum malaria. Trends Parasitol 33:353–363. https://doi.org/10.1016/j.pt.2017.01.004.
4. Duru V, Witkowski B, Menard D. 2016. *Plasmodium falciparum* resistance to artemisinin derivatives and piperaquine: a major challenge for malaria elimination in Cambodia. Am J Trop Med Hyg 95:1228–1238. https://doi.org/10.4269/ajtmh.16-0234.
5. Bachovchin DA, Cravatt BF. 2012. The pharmacological landscape and therapeutic potential of serine hydrolases. Nat Rev Drug Discov 11:52–68. https://doi.org/10.1038/nrd3620.
6. Long JZ, Cravatt BF. 2011. The metabolic serine hydrolases and their functions in mammalian physiology and disease. Chem Rev 111:6022–6063. https://doi.org/10.1021/cr200075y.
7. Aurrecoechea C, Brestelli J, Brunk BP, Dommer J, Fischer S, Gajria B, Gao X, Gingle A, Grant G, Harb OS, Heiges M, Innamorato F, Iodice J, Kissinger JC, Kraemer E, Li W, Miller JA, Nayak V, Pennington C, Pinney DF, Roos DS, Ross C, Stoeckert CJ, Jr, Treatman C, Wang H. 2009. PlasmoDB: a functional genomic database for malaria parasites. Nucleic Acids Res 37:D539–D543. https://doi.org/10.1093/nar/gkn814.
8. Niphakis MJ, Cravatt BF. 2014. Enzyme inhibitor discovery by activity-based protein profiling. Annu Rev Biochem 83:341–377. https://doi.org/10.1146/annurev-biochem-060713-035708.
9. Liu Y, Patricelli MP, Cravatt BF. 1999. Activity-based protein profiling: the serine hydrolases. Proc Natl Acad Sci U S A 96:14694–14699. https://doi.org/10.1073/pnas.96.26.14694.
10. Patricelli MP, Giang DK, Stamp LM, Burbaum JJ. 2001. Direct visualization of serine hydrolase activities in complex proteomes using fluorescent active site-directed probes. Proteomics 1:1067–1071. https://doi.org/10.1002/1615-9861(200109)1:9<1067::AID-PROT1067>3.0.CO;2-4.
11. Fujino T, Tada T, Hosaka T, Beppu M, Kikugawa K. 2000. Presence of oxidized protein hydrolase in human cell lines, rat tissues, and human/rat plasma. J Biochem 127:307–313. https://doi.org/10.1093/oxfordjournals.jbchem.a022608.
12. Jones WM, Manning JM. 1985. Acylpeptide hydrolase activity from erythrocytes. Biochem Biophys Res Commun 126:933–940. https://doi.org/10.1016/0006-291X(85)90275-X.
13. Schonberger OL, Tschesche H. 1981. N-acetylalanine aminopeptidase, a new enzyme from human erythrocytes. Hoppe-Seylers Z Physiol Chem 362:865–873. https://doi.org/10.1515/bchm2.1981.362.2.865.
14. Witheiler J, Wilson DB. 1972. The purification and characterization of a novel peptidase from sheep red cells. J Biol Chem 247:2217–2221.
15. Tsunasawa S, Narita K, Ogata K. 1975. Purification and properties of acylamino acid-releasing enzyme from rat liver. J Biochem 77:89–102.
16. Radhakrishna G, Wold F. 1989. Purification and characterization of an N-acylaminoacyl-peptide hydrolase from rabbit muscle. J Biol Chem 264:11076–11081.
17. Gade W, Brown JL. 1978. Purification and partial characterization of alpha-N-acylpeptide hydrolase from bovine liver. J Biol Chem 253:5012–5018.
18. Fujino T, Kojima M, Beppu M, Kikugawa K, Yasuda H, Takahashi K. 2000. Identification of the cleavage sites of oxidized protein that are susceptible to oxidized protein hydrolase (OPH) in the primary and tertiary structures of the protein. J Biochem 127:1087–1093. https://doi.org/10.1093/oxfordjournals.jbchem.a022702.

19. Yamin R, Zhao C, O'Connor PB, McKee AC, Abraham CR. 2009. Acyl peptide hydrolase degrades monomeric and oligomeric amyloid-beta peptide. Mol Neurodegener 4:33. https://doi.org/10.1186/1750-1326-4-33.
20. Perrier J, Durand A, Giardina T, Puigserver A. 2005. Catabolism of intracellular N-terminal acetylated proteins: involvement of acylpeptide hydrolase and acylase. Biochimie 87:673–685. https://doi.org/10.1016/j.biochi.2005.04.002.
21. Adibekian A, Martin BR, Wang C, Hsu KL, Bachovchin DA, Niessen S, Hoover H, Cravatt BF. 2011. Click-generated triazole ureas as ultrapotent, in vivo-active serine hydrolase inhibitors. Nat Chem Biol 7:469–478. https://doi.org/10.1038/nchembio.579.
22. Palmieri G, Bergamo P, Luini A, Ruvo M, Gogliettino M, Langella E, Saviano M, Hegde RN, Sandomenico A, Rossi M. 2011. Acylpeptide hydrolase inhibition as targeted strategy to induce proteasomal down-regulation. PLoS One 6:e25888. https://doi.org/10.1371/journal.pone.0025888.
23. Shimizu K, Kiuchi Y, Ando K, Hayakawa M, Kikugawa K. 2004. Coordination of oxidized protein hydrolase and the proteasome in the clearance of cytotoxic denatured proteins. Biochem Biophys Res Commun 324:140–146. https://doi.org/10.1016/j.bbrc.2004.08.231.
24. Beaumelle BD, Vial HJ, Philippot JR. 1987. Reevaluation, using marker enzymes, of the ability of saponin and ammonium chloride to free Plasmodium from infected erythrocytes. J Parasitol 73:743–748. https://doi.org/10.2307/3282405.
25. Jones WM, Scaloni A, Bossa F, Popowicz AM, Schneewind O, Manning JM. 1991. Genetic relationship between acylpeptide hydrolase and acylase, two hydrolytic enzymes with similar binding but different catalytic specificities. Proc Natl Acad Sci U S A 88:2194–2198. https://doi.org/10.1073/pnas.88.6.2194.
26. Bonday ZQ, Dhanasekaran S, Rangarajan PN, Padmanaban G. 2000. Import of host δ-aminolevulinate dehydratase into the malarial parasite: identification of a new drug target. Nat Med 6:898–903. https://doi.org/10.1038/78659.
27. Yeh E, DeRisi JL. 2011. Chemical rescue of malaria parasites lacking an apicoplast defines organelle function in blood-stage *Plasmodium falciparum*. PLoS Biol 9:e1001138. https://doi.org/10.1371/journal.pbio.1001138.
28. Dahl EL, Rosenthal PJ. 2007. Multiple antibiotics exert delayed effects against the *Plasmodium falciparum* apicoplast. Antimicrob Agents Chemother 51:3485–3490. https://doi.org/10.1128/AAC.00527-07.
29. Bennett TN, Kosar AD, Ursos LM, Dzekunov S, Singh Sidhu AB, Fidock DA, Roepe PD. 2004. Drug resistance-associated pfCRT mutations confer decreased *Plasmodium falciparum* digestive vacuolar pH. Mol Biochem Parasitol 133:99–114. https://doi.org/10.1016/j.molbiopara.2003.09.008.
30. Klonis N, Tan O, Jackson K, Goldberg D, Klemba M, Tilley L. 2007. Evaluation of pH during cytostomal endocytosis and vacuolar catabolism of hemoglobin in *Plasmodium falciparum*. Biochem J 407:343–354. https://doi.org/10.1042/BJ20070934.
31. Fairfield AS, Meshnick SR, Eaton JW. 1983. Malaria parasites adopt host cell superoxide dismutase. Science 221:764–766. https://doi.org/10.1126/science.6348944.
32. Koncarevic S, Rohrbach P, Deponte M, Krohne G, Prieto JH, Yates IIJ, Rahlfs S, Becker K. 2009. The malarial parasite *Plasmodium falciparum* imports the human protein peroxiredoxin 2 for peroxide detoxification. Proc Natl Acad Sci U S A 106:13323–13328. https://doi.org/10.1073/pnas.0905387106.
33. Elliott DA, McIntosh MT, Hosgood HD, Chen S, Zhang G, Baevova P, Joiner KA. 2008. Four distinct pathways of hemoglobin uptake in the malaria parasite *Plasmodium falciparum*. Proc Natl Acad Sci U S A 105:2463–2468. https://doi.org/10.1073/pnas.0711067105.
34. Lazarus MD, Schneider TG, Taraschi TF. 2008. A new model for hemoglobin ingestion and transport by the human malaria parasite *Plasmodium falciparum*. J Cell Sci 121:1937–1949. https://doi.org/10.1242/jcs.023150.
35. Abu Bakar N, Klonis N, Hanssen E, Chan C, Tilley L. 2010. Digestive-vacuole genesis and endocytic processes in the early intraerythrocytic stages of *Plasmodium falciparum*. J Cell Sci 123:441–450. https://doi.org/10.1242/jcs.061499.
36. Hanssen E, Knoechel C, Dearnley M, Dixon MW, Le Gros M, Larabell C, Tilley L. 2012. Soft X-ray microscopy analysis of cell volume and hemoglobin content in erythrocytes infected with asexual and sexual stages of *Plasmodium falciparum*. J Struct Biol 177:224–232. https://doi.org/10.1016/j.jsb.2011.09.003.
37. Goldberg DE. 2005. Hemoglobin degradation. Curr Top Microbiol Immunol 295:275–291.
38. Scaloni A, Ingallinella P, Andolfo A, Jones W, Marino G, Manning JM. 1999. Structural investigations on human erythrocyte acylpeptide hydrolase by mass spectrometric procedures. J Protein Chem 18:349–360. https://doi.org/10.1023/A:1021047730831.
39. Sharma KK, Ortwerth BJ. 1993. Bovine lens acylpeptide hydrolase. Purification and characterization of a tetrameric enzyme resistant to urea denaturation and proteolytic inactivation. Eur J Biochem 216:631–637. https://doi.org/10.1111/j.1432-1033.1993.tb18183.x.
40. Durand A, Villard C, Giardina T, Perrier J, Juge N, Puigserver A. 2003. Structural properties of porcine intestine acylpeptide hydrolase. J Protein Chem 22:183–191. https://doi.org/10.1023/A:1023431215558.
41. Chongcharoen K, Sharma KK. 1998. Characterization of trypsin-modified bovine lens acylpeptide hydrolase. Biochem Biophys Res Commun 247:136–141. https://doi.org/10.1006/bbrc.1998.8747.
42. McFadden GI, Roos DS. 1999. Apicomplexan plastids as drug targets. Trends Microbiol 7:328–333. https://doi.org/10.1016/S0966-842X(99)01547-4.
43. Bannister LH, Hopkins JM, Margos G, Dluzewski AR, Mitchell GH. 2004. Three-dimensional ultrastructure of the ring stage of *Plasmodium falciparum*: evidence for export pathways. Microsc Microanal 10:551–562. https://doi.org/10.1017/S1431927604040917.
44. Ringrose JH, van Solinge WW, Mohammed S, O'Flaherty MC, van Wijk R, Heck AJR, Slijper M. 2008. Highly efficient depletion strategy for the two most abundant erythrocyte soluble proteins improves proteome coverage dramatically. J Proteome Res 7:3060–3063. https://doi.org/10.1021/pr8001029.
45. Lange PF, Huesgen PF, Nguyen K, Overall CM. 2014. Annotating N termini for the human proteome project: N termini and Nalpha-acetylation status differentiate stable cleaved protein species from degradation remnants in the human erythrocyte proteome. J Proteome Res 13:2028–2044. https://doi.org/10.1021/pr401191w.
46. Lin KT, Deutsch HF. 1973. Human carbonic anhydrases. XI. The complete primary structure of carbonic anhydrase B. J Biol Chem 248:1885–1893.
47. Bryk AH, Wiśniewski JR. 2017. Quantitative analysis of human red blood cell proteome. J Proteome Res 16:2752–2761. https://doi.org/10.1021/acs.jproteome.7b00025.
48. Roux-Dalvai F, Gonzalez de Peredo A, Simo C, Guerrier L, Bouyssie D, Zanella A, Citterio A, Burlet-Schiltz O, Boschetti E, Righetti PG, Monsarrat B. 2008. Extensive analysis of the cytoplasmic proteome of human erythrocytes using the peptide ligand library technology and advanced mass spectrometry. Mol Cell Proteomics 7:2254–2269. https://doi.org/10.1074/mcp.M800037-MCP200.
49. Dalal S, Klemba M. 2007. Roles for two aminopeptidases in vacuolar hemoglobin catabolism in *Plasmodium falciparum*. J Biol Chem 282:35978–35987. https://doi.org/10.1074/jbc.M703643200.
50. Klemba M, Gluzman I, Goldberg DE. 2004. A *Plasmodium falciparum* dipeptidyl aminopeptidase I participates in vacuolar hemoglobin degradation. J Biol Chem 279:43000–43007. https://doi.org/10.1074/jbc.M408123200.
51. Jones WM, Manning JM. 1988. Substrate specificity of an acylaminopeptidase that catalyzes the cleavage of the blocked amino termini of peptides. Biochim Biophys Acta 953:357–360. https://doi.org/10.1016/0167-4838(88)90045-3.
52. Lambros C, Vanderberg JP. 1979. Synchronization of *Plasmodium falciparum* erythrocytic stages in culture. J Parasitol 65:418–420. https://doi.org/10.2307/3280287.
53. Smilkstein M, Sriwilaijaroen N, Kelly JX, Wilairat P, Riscoe M. 2004. Simple and inexpensive fluorescence-based technique for high-throughput antimalarial drug screening. Antimicrob Agents Chemother 48:1803–1806. https://doi.org/10.1128/AAC.48.5.1803-1806.2004.
54. Ragheb D, Dalal S, Bompiani KM, Ray WK, Klemba M. 2011. Distribution and biochemical properties of an M1-family aminopeptidase in *Plasmodium falciparum* indicate a role in vacuolar hemoglobin catabolism. J Biol Chem 286:27255–27265. https://doi.org/10.1074/jbc.M111.225318.
55. Istvan ES, Mallari JP, Corey VC, Dharia NV, Marshall GR, Winzeler EA, Goldberg DE. 2017. Esterase mutation is a mechanism of resistance to antimalarial compounds. Nat Commun 8:14240. https://doi.org/10.1038/ncomms14240.